ORIGINAL RESEARCH ARTICLE

Experimental Investigation and Thermodynamic Description of Phase Equilibria in the Al-Cr-Mo Ternary System

Cuiping Wang[1,2] · Xiaodong Chen[1,2] · Xi Wu[1,2] · Yixiong Huang[1,2] ·
Yihui Guo[1,2] · Shuiyuan Yang[1,2] · Yong Lu[1,2] · Xingjun Liu[3]

Abstract The isothermal sections of the Al-Cr-Mo ternary system at 1200 and 1000 °C were experimentally determined based on microstructure and phase constituents from the equilibrated alloys employing electron probe microanalysis, scanning electron microscopy, and x-ray diffraction. A new ternary compound phase named η with AlTi$_3$-type crystal structure covering a composition range with $\sim$ 75 at.% Al was detected in these two investigated isothermal sections in the present work. Based on the experimental results and the published data of the three binary sub-systems, a thermodynamic description for the Al-Cr-Mo system was carried out using the CALPHAD (CALculation of PHAse Diagrams) method. The newly detected ternary phase η was modeled by a two-sublattice model of (Al)$_3$(Al,Cr,Mo)$_1$. A set of reliable thermodynamic parameters of the Al-Cr-Mo system was obtained, which are in satisfactory agreement with the experimental data. Based on the obtained thermodynamic parameters, much information related to the stable vertical sections, isothermal sections, liquidus projection, and miscibility

gap of the bcc phase were predicted in the present work. The present work can provide essential experimental and thermodynamic data for the establishment of the Ni-Al-Cr-Mo based alloy database.

1 Introduction

Ni-based superalloys have been widely used as high-temperature structural materials in contemporary aerospace and gas turbine industries, due to their exceptional high-temperature microstructure stability, mechanical properties, fatigue resistance, and thermal corrosion resistance.[1–5] Advanced Ni-based superalloys generally contain generous levels of alloying elements to achieve outstanding comprehensive properties at elevated temperatures. Al is considered as an indispensable alloying element for Ni-based superalloys because it can not only form the precipitation strengthening phase γ'-Ni$_3$Al with the L1$_2$ structure, but also form the dense Al$_2$O$_3$ to enhance oxidation resistance.[6–8] Cr can significantly ameliorate the high-temperature oxidation and corrosion resistance of Ni-based superalloys by forming the Cr$_2$O$_3$ film on the alloy surface.[7,9,10] In addition, an appropriate amount of Cr content is conducive to improving the stress-rupture property of Ni-based superalloys.[11] The addition of Mo can increase the lattice parameter of the γ phase and enhance the creep performance of the alloys.[6,9,12] Nevertheless, if the concentrations of Cr and Mo are too large, the brittle topologically close-packed (TCP) phases will be present while using at high temperatures or applying stress,

✉ Yihui Guo
gyh@xmu.edu.cn

✉ Yong Lu
luyong@xmu.edu.cn

1   College of Materials, and Fujian Key Laboratory of Surface and Interface Engineering for High Performance Materials, Xiamen University, Xiamen 361005, People's Republic of China

2   Xiamen Key Laboratory of High Performance Metals and Materials, Xiamen University, Xiamen 361005, People's Republic of China

3   School of Materials Science and Engineering, and Institute of Materials Genome & Big Data, Harbin Institute of Technology, Shenzhen 518055, People's Republic of China

which is detrimental to high-temperature service.[13,14] Therefore, to design Ni-based superalloys with long-term microstructural stability at elevated temperatures, reliable knowledge of phase relationships in Ni-Al-Cr-Mo systems is a prerequisite.

Several works have been done to investigate the phase relations of the ternary Al-Cr-Ni,[15,16] Cr-Mo-Ni,[17,18] and Al-Mo-Ni[19–21] systems. However, as an important subsystem, phase information of the Al-Cr-Mo ternary system has not attracted much attention. The only experimental data was reported in 1964, Raman et al.[22] prepared five as-cast Al-Cr-Mo alloys containing 33.3 at.% Al by arc melting, and determined the dominating solidified bcc phase through x-ray diffraction (XRD). The thermodynamic calculations of the Al-Cr-Mo system were first performed by Kaufman et al.[23], which was an extrapolation from the respective binary systems. Furthermore, Peng et al.[18,24] assessed the ternary interaction parameter of the liquid phase in the Al-Cr-Mo system to fit the experimental data of the Ni-Al-Cr-Mo quaternary system. However, no ternary Al-Cr-Mo system experimental data could be located for comparison with the calculated results. Therefore, a systematic investigation of the phase equilibria determination and thermodynamic description in the Al-Cr-Mo ternary system over the whole composition range is of great significance.

The objective of the present work is to experimentally investigate the phase equilibria in the Al-Cr-Mo ternary system at 1200 and 1000 °C, and to carry out the thermodynamic assessment of the Al-Cr-Mo ternary system based on the experimental data utilizing CALPHAD technique. The obtained experimental data and thermodynamic parameters are expected to support establishing the Ni-Al-Cr-Mo based superalloy database.

2 Experimental Procedure

A series of Al-Cr-Mo alloys with different nominal compositions were prepared using pure bulk metals Al (99.99 wt.%), Cr (99.99 wt.%), and Mo (99.99 wt.%) as starting materials. The prepared metals were put into an arc melting furnace with a vacuum of 6.6×10^{-3} Pa and subsequently filled with high-purity argon as a protective gas. The ingots were inverted and remelted at least four times to ensure a weight loss below 0.50%, to achieve compositional uniformity. The weight of each ingot was about 15 g.

Afterward, the ingots were cut into small pieces by wire-cut electrical discharge machining. Then the specimens, wrapped with Nb foil, were put into a quartz tube to avoid contamination of the specimens. The appropriate amount of argon was filled to balance the pressure inside and outside the quartz tube during heat treatment. Most of the

specimens were annealed at 1200 °C for 30 days or 1000 °C for 60 days, except for the specimens containing the liquid phase, which were annealed at 1200 °C for 20 minutes or 1000 °C for 30 minutes. After heat treatment, the specimens were quenched immediately in ice water to maintain the phase equilibria at the annealing temperature.

After standard metallographic preparation, the microstructure and phase constituents of the equilibrated alloys were investigated by backscattered electron (BSE) imaging and an electron probe microanalysis (EPMA) (JXA-8100R) under the conditions of 20.0 kV accelerating voltage and 1.0×10^{-8} A probe current. The composition of the samples containing the liquid phase was determined by scanning electron microscopy (SEM) (SU-70) with an energy dispersive spectroscopy (EDS). Then the samples were cut and mashed into finer particles (around 75 μm) with a stainless-steel mortar, and after sieving the finer particles into an agate mortar they were further finely ground to around 20 μm. It was then held under vacuum for a few minutes for stress relief annealing. The powder XRD measurement was carried out to analyze the crystal structure of the alloys using CuK_α radiation at 40.0 kV and 40 mA.

3 Thermodynamic Models

The Gibbs free energy functions describing pure Al, Cr, and Mo are taken from the Scientific Group Thermodata Europe (SGTE) database compiled by Dinsdale.[25] The thermodynamic parameters of the Al-Cr, Al-Mo, and Cr-Mo binary systems reported by Liang et al.[26], Du et al.[27], and Frisk et al.[28] are accepted in the present work. The calculated binary phase diagrams are presented in Fig. 1. The structures and the used models of all phases in the Al-Cr-Mo ternary system are listed in Table 1.

3.1 Solution Phases

The sub-regular solution model is used to describe the molar Gibbs free energy of the liquid, fcc, and bcc solution phases, defined as:

$$G_m^\varphi = \sum_{i=Al,Cr,Mo} x_i {}^0G_i^\varphi + RT \sum_{i=Al,Cr,Mo} x_i \ln x_i^\varphi + {}^E G_m^\varphi$$

(Eq 1)

where x_i is the molar fractions of the pure element i (Al, Cr, or Mo) and ${}^0G_i^\varphi$ refers to their corresponding molar Gibbs energies in the φ (liquid, fcc, or bcc) phase. ${}^E G_m^\varphi$ is the excess Gibbs free energy, which is expressed by the Redlich-Kister polynomials[29] and Hillert[30] as follows:
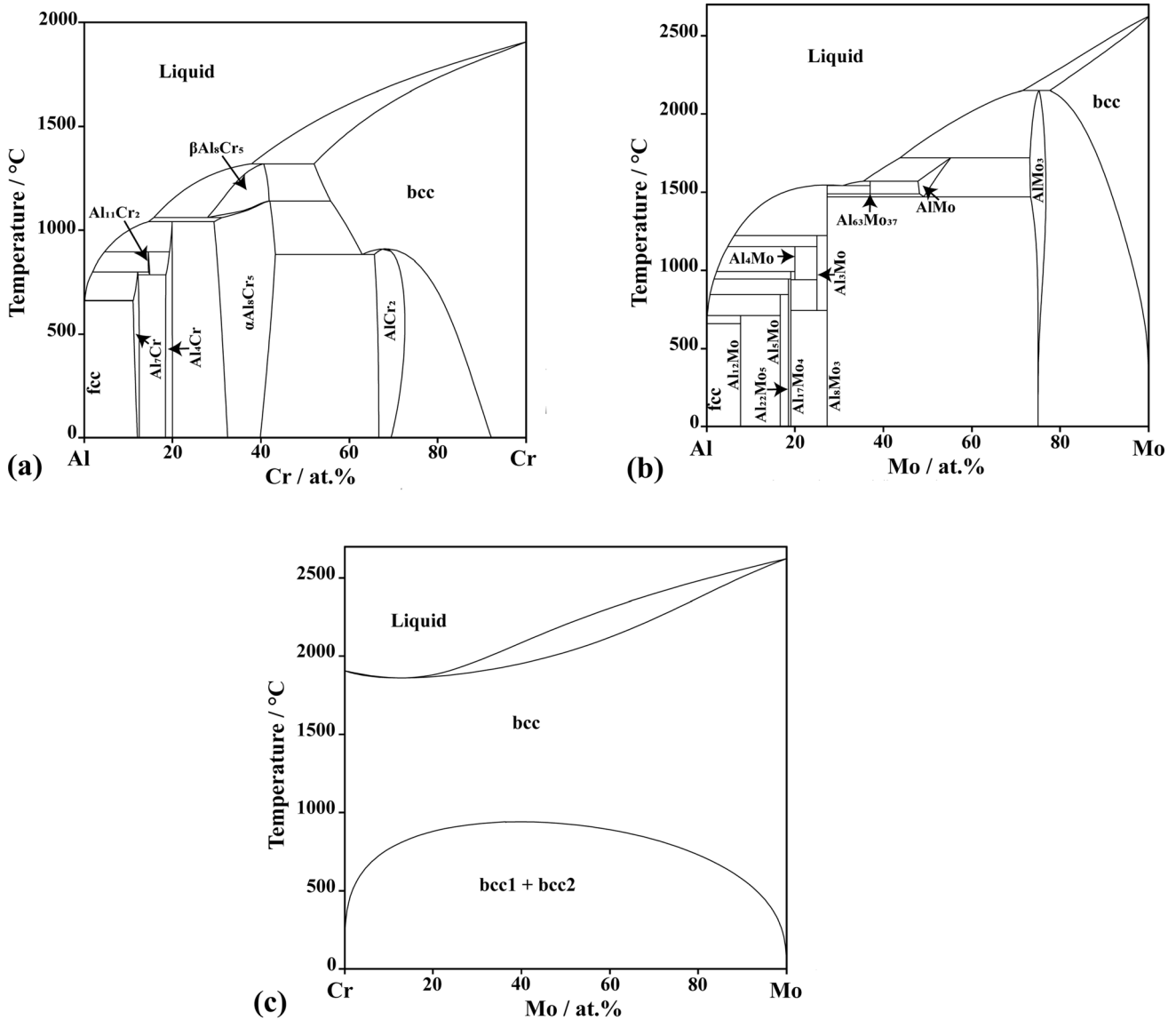
20

J. Phase Equilib. Diffus. (2024) 45:18–35

Fig. 1 Calculated binary phase diagrams in the Al-Cr-Mo ternary system: (a) Al-Cr system,[26] (b) Al-Mo system,[27] and (c) Cr-Mo system[28]

$$^{E}G^{\varphi} = x_{Al}x_{Cr}L_{Al,Cr}^{\varphi} + x_{Al}x_{Mo}L_{Al,Mo}^{\varphi} + x_{Cr}x_{Mo}L_{Cr,Mo}^{\varphi}$$
$$+ x_{Al}x_{Cr}x_{Mo}L_{Al,Cr,Mo}^{\varphi} \qquad \text{(Eq 2)}$$

$$L_{i,j}^{\varphi} = \sum_{m=0}^{n} {}^{m}L_{i,j}^{\varphi}(x_i - x_j)^m \qquad \text{(Eq 3)}$$

$$L_{Al,Cr,Mo}^{\varphi} = x_{Al}{}^{0}L_{Al,Cr,Mo}^{\varphi} + x_{Cr}{}^{1}L_{Al,Cr,Mo}^{\varphi} + x_{Mo}{}^{2}L_{Al,Cr,Mo}^{\varphi}$$
$$\text{(Eq 4)}$$

where $L_{i,j}^{\varphi}$ is the interaction parameter in the $i-j$ (any two of Al, Cr, or Mo) binary system. The ternary parameters, $^{0}L_{Al,Cr,Mo}^{\varphi}$, $^{1}L_{Al,Cr,Mo}^{\varphi}$, and $^{2}L_{Al,Cr,Mo}^{\varphi}$, will be optimized in the present work.

3.2 Intermetallic Compounds

In the literature,(Ref 26,27) the intermetallic compounds Al₇Cr, Al₄Cr, αAl₈Cr₅, βAl₈Cr₅, AlCr₂, and AlMo₃ were described by two-sublattice solution model. According to the model, the molar Gibbs free energy of these phases in the Al-Cr-Mo ternary system is expressed as follows:

$$G_m^{\lambda} = \sum_i y_i' \sum_j y_j''{}^{0}G_{i:j}^{\lambda}$$
$$+ RT\left(a\sum_i y_i' ln y_i' + b\sum_j y_j'' ln y_j''\right) + {}^{E}G_m^{\lambda} \qquad \text{(Eq 5)}$$

where the site fraction y_*^n denote the composition of the respective sublattice n, a and b are their stoichiometric coefficients. $^{0}G_{i:j}^{\lambda}$ are the compound energies of the respective end-members of the λ phase, and $^{E}G_m^{\lambda}$ is the

Table 1 Crystal structures and thermodynamic models of all phases in the Al-Cr-Mo system

Phase	Strukturbericht designation	Pearson symbol	Space group	Prototype	Thermodynamic model
liquid	…	…	…	…	$(Al,Cr,Mo)_1$
fcc	$A1$	$cF4$	$Fm\overline{3}m$	Cu	$(Al,Cr,Mo)_1$
bcc	$A2$	$cI2$	$Im\overline{3}m$	W	$(Al,Cr,Mo)_1$
Al_7Cr	…	$mC104$	$C2/m$	$Al_{45}Cr_7$	$(Al)_7(Al,Cr)_1$
$Al_{11}Cr_2$	…	$mP48$	$P2$	…	$(Al)_{11}(Al,Cr)_2$
Al_4Cr	…	$hR574$	$P6_3/mmc$	μAl_4Mn	$(Al)_4(Al,Cr)_1$
αAl_8Cr_5	$D8_{10}$	$hR26$	$R\overline{3}m$	Al_8Cr_5	$(Al,Cr,Mo)_8(Al,Cr,Mo)_5$
βAl_8Cr_5	…	$cI52$	$I4\overline{3}m$	Zn_8Cu_5	$(Al,Cr,Mo)_8(Al,Cr,Mo)_5$
$AlCr_2$	$C11_b$	$tI6$	$I4/mmm$	$MoSi_2$	$(Al,Cr)_1(Al,Cr)_2$
$Al_{12}Mo$	…	$cI26$	$Im\overline{3}$	$Al_{12}W$	$(Al)_{12}(Mo)_1$
Al_5Mo	…	$hP12$	$P6_3$	Al_5W	$(Al)_5(Mo)_1$
$Al_{22}Mo_5$	…	$oF216$	$Fdd2$	…	$(Al)_{22}(Mo)_5$
$Al_{17}Mo_4$	…	$mC84$	$C2$	…	$(Al)_{17}(Mo)_4$
Al_4Mo	…	$mC30$	Cm	Al_4W	$(Al)_4(Mo)_1$
Al_3Mo	…	$mC32$	Cm	…	$(Al)_3(Mo)_1$
Al_8Mo_3	…	$mC22$	$C2/m$	…	$(Al)_8(Cr,Mo)_3$
$Al_{63}Mo_{37}$	…	…	…	…	$(Al)_{63}(Mo)_{37}$
AlMo	$A2$	$cI2$	$Im\overline{3}m$	W	$(Al,Cr,Mo)_1$
$AlMo_3$	$A15$	$cP8$	$Pm\overline{3}n$	Cr_3Si	$(Al,Mo)_1(Al,Cr,Mo)_3$

excess Gibbs energy which is given by the following expression:

$$^E G_m^\lambda = \sum_{i,k} \sum_j \left[y_i\prime y_k\prime y_j'' \left(\sum_{n=0}^n {}^n L_{i,k:j}^\lambda (y_i\prime - y_k\prime)^n \right) \right]$$
$$+ \sum_i \sum_{j,k} \left[y_i\prime y_j'' y_k'' \left(\sum_{n=0}^n {}^n L_{i:j,k}^\lambda (y_j\prime - y_k\prime)^n \right) \right]$$
$$+ y_i\prime y_{Al}'' y_{Cr}'' y_{Mo}'' {}^n L_{i:Al,Cr,Mo}^\lambda + y_{Al}\prime y_{Cr}\prime y_{Mo}\prime y_i'' {}^n L_{Al,Cr,Mo:i}^\lambda$$

(Eq 6)

The interaction parameters, $^n L_{i,j:k}^\lambda$, $^n L_{i:j,k}^\lambda$, $^n L_{i:Al,Cr,Mo}^\lambda$, and $^n L_{Al,Cr,Mo:i}^\lambda$, which can be expressed as $a + bT$, will be optimized in the present work.

The compound AlMo with A2 structure was treated as the same phase as bcc with the same Gibbs energy function as Eq. 1.[27]

3.3 Stoichiometric Compounds

The $Al_{12}Mo$, Al_5Mo, $Al_{22}Mo_5$, $Al_{17}Mo_4$, Al_3Mo, Al_8Mo_3, and $Al_{63}Mo_{37}$ phases were treated as stoichiometric compounds in the literature.[27] The Gibbs energy per mole of formula unit Al_mMo_n is described as:

$$G_m^{Al_mMo_n} = m\,^0 G_{Al}^{HSER} + n\,^0 G_{Mo}^{HSER} + a' + b'T$$

(Eq 7)

where $^0 G_{Al}^{HSER}$ and $^0 G_{Mo}^{HSER}$ are the molar Gibbs energy of fcc Al and bcc Mo referred to the enthalpy of the standard element reference (HSER) at 25 °C and 10^5 Pa, respectively. The parameters a′ and b′ will be evaluated in the present work.

4 Results and Discussion

4.1 Experimental Determination

In the following sections, some representative BSE images and XRD indexing results of the Al-Cr-Mo ternary alloys annealed at 1200 and 1000 °C are shown to illustrate their phase equilibria.

4.1.1 Phase Equilibria with the Newly Detected η Phase

The BSE image of the $Al_{74}Cr_{14}Mo_{12}$ (at.%) alloy annealed at 1200 °C for 20 minutes in Fig. 2(a) shows the coexistence of three phases. The gray regions and dark eutectic-like regions were identified to be the βAl_8Cr_5 and solidified liquid phases, respectively. Furthermore, one light and lamellar region in microstructure was observed and presumed to be an unidentified ternary compound (denoted as η later). In the corresponding XRD pattern (Fig. 3(a)), the characteristic peaks of the βAl_8Cr_5 and Al-rich (liquid)
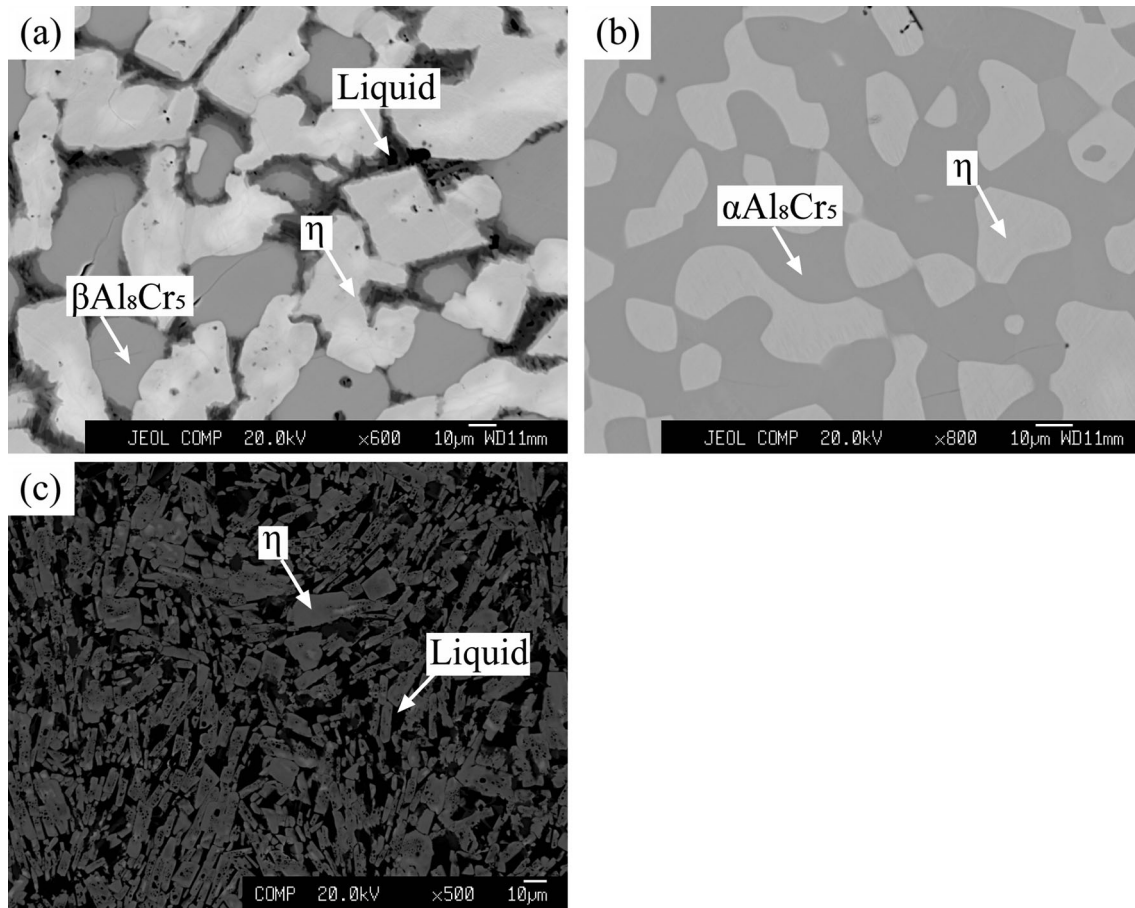
22

J. Phase Equilib. Diffus. (2024) 45:18–35

Fig. 2 BSE images of the typical Al-Cr-Mo ternary alloys: (a) the $Al_{74}Cr_{14}Mo_{12}$ (at.%) alloy annealed at 1200 °C for 20 minutes; (b) the $Al_{73}Cr_{21}Mo_6$ (at.%) alloy annealed at 1000 °C for 60 days; and (c) the $Al_{81}Cr_{11}Mo_8$ (at.%) alloy annealed at 1000 °C for 30 minutes
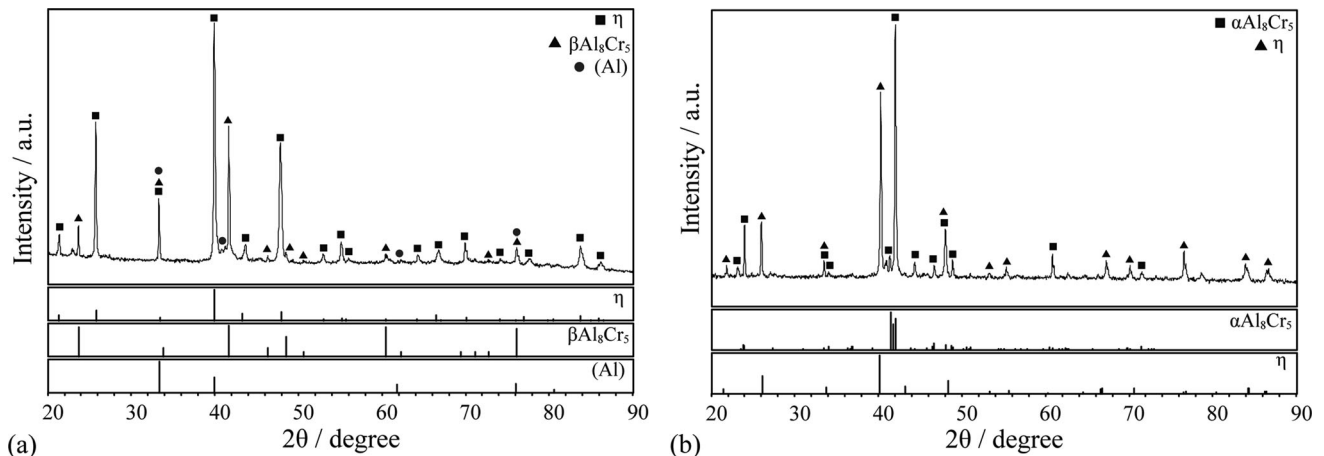

Fig. 3 X-ray diffraction patterns obtained from typical Al-Cr-Mo ternary alloys: (a) the $Al_{74}Cr_{14}Mo_{12}$ (at.%) alloy annealed at 1200 °C for 20 minutes and (b) the $Al_{73}Cr_{21}Mo_6$ (at.%) alloy annealed at 1000 °C for 60 days

phases are well distinguished, while the remaining peaks were assumed to be from the η phase. The crystal structure of the newly detected ternary compound is related to AlTi$_3$-type space group according to the Powder Diffraction File (PDF) cards. The η phase was also observed in other alloys

at 1000 °C. As shown in Fig. 2(b), two different phase contrasts are well distinguished for the 1000 °C-annealed $Al_{73}Cr_{21}Mo_6$ (at.%) alloy. The gray phase was readily determined as the αAl_8Cr_5 phase, while the light one was identified as the η phase. The XRD result confirmed the
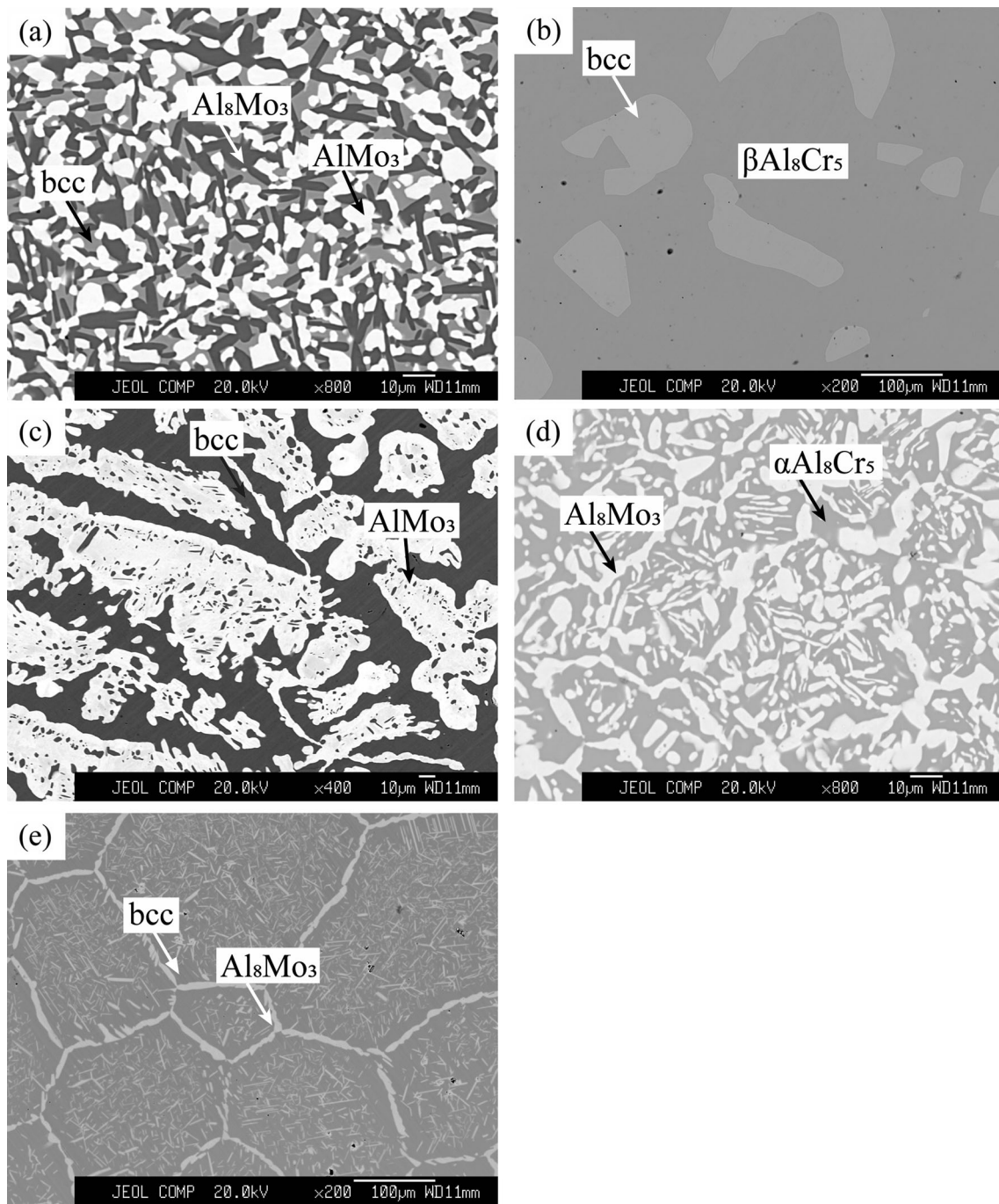
Fig. 4 BSE images of the typical Al-Cr-Mo ternary alloys: (a) the $Al_{40}Cr_{10}Mo_{50}$ (at.%) alloy annealed at 1200 °C for 30 days; (b) the $Al_{50}Cr_{40}Mo_{10}$ (at.%) alloy annealed at 1200 °C for 30 days; (c) the $Al_{40}Cr_{30}Mo_{30}$ (at.%) alloy annealed at 1200 °C for 30 days; (d) the $Al_{65}Cr_{25}Mo_{10}$ (at.%) alloy annealed at 1000 °C for 60 days; and (e) the $Al_{50}Cr_{36}Mo_{14}$ (at.%) alloy annealed at 1000 °C for 60 days

24

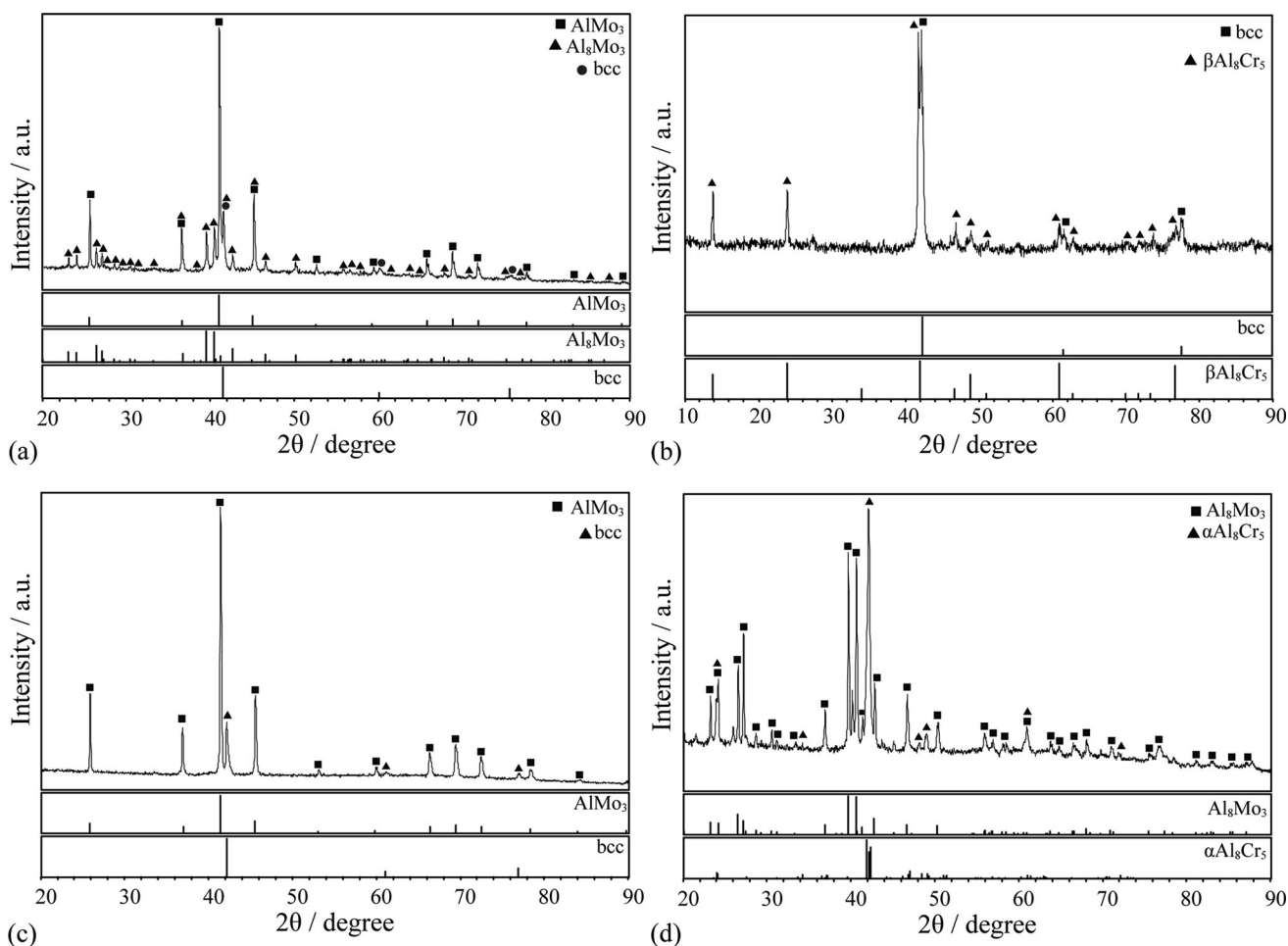J. Phase Equilib. Diffus. (2024) 45:18–35

Fig. 5 X-ray diffraction patterns obtained from typical Al-Cr-Mo ternary alloys: (a) the $Al_{40}Cr_{10}Mo_{50}$ (at.%) alloy annealed at 1200 °C for 30 days; (b) the $Al_{50}Cr_{40}Mo_{10}$ (at.%) alloy annealed at 1200 °C for 30 days; (c) the $Al_{40}Cr_{30}Mo_{30}$ (at.%) alloy annealed at 1200 °C for 30 days; and (d) the $Al_{65}Cr_{25}Mo_{10}$ (at.%) alloy annealed at 1000 °C for 60 days

crystal structures of the two phases. The diffraction peaks of the two phases, marked by different symbols, are shown in Fig. 3(b). In addition, the two-phase microstructure of the dark solidified liquid and gray η phases coexist in the $Al_{81}Cr_{11}Mo_8$ (at.%) alloy annealed at 1000 °C for 30 minutes, as shown in Fig. 2(c).

4.1.2 Equilibria of the Other Phases

For the $Al_{40}Cr_{10}Mo_{50}$ (at.%) alloy annealed at 1200 °C for 30 days, the three-phase microstructure of bcc (gray), Al_8Mo_3 phase (dark), and $AlMo_3$ phase (light) is apparent, as shown in Fig. 4(a), and the characteristic peaks of three phases are identified in Fig. 5(a). The BSE image (Fig. 4(b)) and XRD result (Fig. 5(b)) show that the $Al_{50}Cr_{40}Mo_{10}$ (at.%) alloy annealed at 1200 °C for 30 days is in a two-phase region and the light and gray regions are bcc and βAl_8Cr_5, respectively. The two-phase equilibrium of dark bcc phase and light $AlMo_3$ phase was identified in the

$Al_{40}Cr_{30}Mo_{30}$ (at.%) alloy annealed at 1200 °C for 30 days, as shown in Fig. 4(c). Furthermore, the two phases were also confirmed by the XRD pattern shown in Fig. 5(c). In Fig. 4(d), a two-phase equilibrium can be seen, with the light Al_8Mo_3 phase and gray αAl_8Cr_5 phase occurring in the $Al_{65}Cr_{25}Mo_{10}$ (at.%) alloy annealed at 1000 °C for 60 days. The corresponding XRD pattern is presented in Fig. 5(d), in which these two different phases are well distinguished. Constituent phases of the $Al_{50}Cr_{36}Mo_{14}$ (at.%) alloy annealed at 1000 °C for 60 days are shown in Fig. 4(e), the light gray phase is Al_8Mo_3 and the dark gray phase is bcc.

The designed nominal alloys and analyzed composition of constituent phases in the Al-Cr-Mo system annealed at 1200 and 1000 °C are summarized in Tables 2 and 3, respectively.

Table 2 Equilibrium compositions of the Al-Cr-Mo ternary system at 1200 °C determined in the present work

Alloys (at.%)	Annealed time	Phase equilibria Phase 1/Phase 2/Phase 3	Composition (at.%)					
			Phase 1		Phase 2		Phase 3	
			Al	Mo	Al	Mo	Al	Mo
$Al_{74}Cr_{14}Mo_{12}$	20 min	$\beta Al_8Cr_5/\eta/$liquid	70.61	6.51	74.80	15.55	84.09	3.31
$Al_{53}Cr_{20}Mo_{27}$	30 days	bcc/Al_8Mo_3	43.53	25.94	72.52	26.55	…	…
$Al_{33}Cr_{37}Mo_{30}$	30 days	bcc/$AlMo_3$	41.80	28.47	26.47	58.26	…	…
$Al_{40}Cr_{30}Mo_{30}$	30 days	bcc/$AlMo_3$	39.64	28.12	26.98	54.79	…	…
$Al_{40}Cr_{48}Mo_{12}$	30 days	bcc	40.15	12.47	…	…	…	…
$Al_{40}Cr_{10}Mo_{50}$	30 days	bcc/Al_8Mo_3/$AlMo_3$	45.02	30.03	72.63	26.23	27.24	61.87
$Al_{69}Cr_{10}Mo_{21}$	30 days	$Al_8Mo_3/\beta Al_8Cr_5$	73.09	25.48	61.63	15.80	…	…
$Al_{60}Cr_{30}Mo_{12}$	30 days	βAl_8Cr_5	58.97	10.63	…	…	…	…
$Al_{50}Cr_{40}Mo_{10}$	30 days	bcc/βAl_8Cr_5	41.87	9.11	57.83	9.72	…	…
$Al_{55}Cr_{35}Mo_{12}$	30 days	bcc/βAl_8Cr_5	42.48	11.44	58.32	11.70	…	…
$Al_{26}Cr_{24}Mo_{50}$	30 days	bcc/$AlMo_3$	30.11	23.82	25.89	53.40	…	…
$Al_{36}Cr_{24}Mo_{40}$	30 days	bcc/$AlMo_3$	43.50	30.18	25.14	62.17	…	…
$Al_{20}Cr_{13}Mo_{67}$	30 days	bcc/$AlMo_3$	10.13	73.17	23.70	65.14	…	…
$Al_{20}Cr_{22}Mo_{58}$	30 days	bcc/$AlMo_3$	9.42	51.72	22.98	60.39	…	…
$Al_{20}Cr_7Mo_{73}$	30 days	bcc/$AlMo_3$	8.80	84.09	22.89	71.30		
$Al_5Cr_3Mo_{92}$	30 days	bcc	4.81	92.15	…	…	…	…
$Al_{40}Cr_8Mo_{52}$	30 days	$Al_8Mo_3/AlMo_3$	73.08	26.53	26.11	65.03	…	…

Table 3 Equilibrium compositions of the Al-Cr-Mo ternary system at 1000 °C determined in the present work

| Alloys (at.%) | Annealed time | Phase equilibria Phase 1/Phase 2/Phase 3 | Composition (at.%) | | | | | |
			Phase 1		Phase 2		Phase 3	
			Al	Mo	Al	Mo	Al	Mo
$Al_{70}Cr_{15}Mo_{15}$	60 days	$\alpha Al_8Cr_5/\eta/Al_8Mo_3$	65.22	5.71	74.75	12.94	72.98	24.69
$Al_{33}Cr_{37}Mo_{30}$	60 days	bcc/$AlMo_3$	38.25	17.01	27.44	47.71	…	…
$Al_{45}Cr_{13}Mo_{42}$	60 days	$Al_8Mo_3/AlMo_3$	73.32	25.91	27.63	51.05	…	…
$Al_{40}Cr_{10}Mo_{50}$	60 days	$Al_8Mo_3/AlMo_3$	73.80	25.80	26.71	54.86	…	…
$Al_{50}Cr_{36}Mo_{14}$	60 days	bcc/Al_8Mo_3	38.10	9.57	73.48	25.21	…	…
$Al_{73}Cr_{21}Mo_6$	60 days	$\alpha Al_8Cr_5/\eta$	71.45	2.77	74.90	10.00	…	…
$Al_{65}Cr_{25}Mo_{10}$	60 days	$Al_8Mo_3/\alpha Al_8Cr_5$	72.81	24.54	63.40	7.55	…	…
$Al_{37}Cr_{47}Mo_{16}$	60 days	bcc	36.57	15.86	…	…	…	…
$Al_{50}Cr_{32}Mo_{18}$	60 days	bcc/Al_8Mo_3	38.38	10.77	72.97	25.98	…	…
$Al_{40}Cr_8Mo_{52}$	60 days	$Al_8Mo_3/AlMo_3$	73.35	26.39	26.53	61.21	…	…
$Al_{36}Cr_{24}Mo_{40}$	60 days	bcc/Al_8Mo_3/$AlMo_3$	37.88	19.07	73.61	25.80	26.54	50.22
$Al_{81}Cr_{11}Mo_8$	30 min	$\eta/$liquid	78.05	11.26	86.79	2.6		
$Al_{20}Cr_{20}Mo_{60}$	60 days	bcc/$AlMo_3$	7.13	70.50	24.05	61.08	…	…
$Al_{26}Cr_{29}Mo_{45}$	60 days	bcc/$AlMo_3$	25.99	13.75	26.06	48.22	…	…
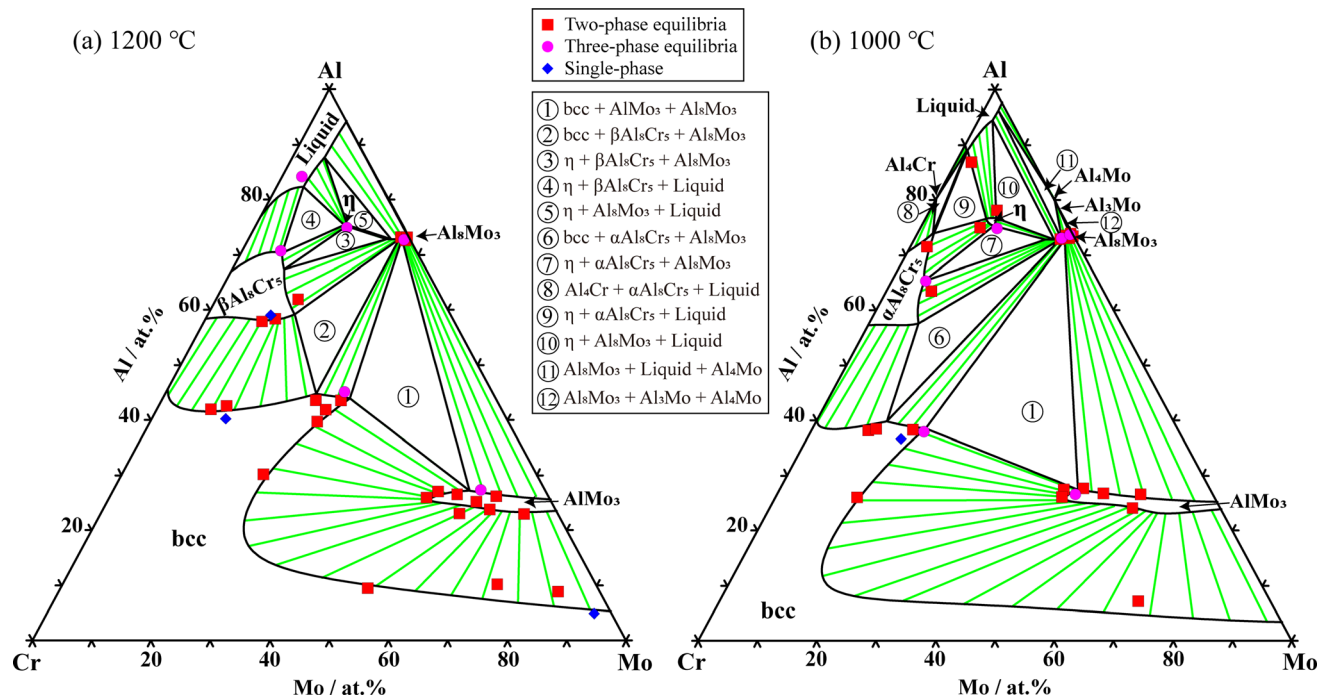
Fig. 6 Calculated isothermal sections of the Al-Cr-Mo system at (a) 1200 °C and (b) 1000 °C with the experimental data determined in the present work

4.2 Thermodynamic Calculation

Based on the experimental data and the published thermodynamic parameters of the Al-Cr,(Ref 26) Al-Mo,(Ref 27) and Cr-Mo(Ref 28) binary systems, a thermodynamic description of the Al-Cr-Mo ternary system was developed. The newly detected ternary compound phase η was modeled by a two-sublattice model of $(Al)_3(Al,Cr,Mo)_1$ according to its crystal structure and homogeneity range. The calculated isothermal sections at 1200 and 1000 °C along with the experimental data marked by different symbols are presented in Fig. 6(a)-(b), where the calculated results are in good agreement with the experimental data. All the thermodynamic parameters optimized in the present work are listed in Table 4.

It can be seen from Fig. 6(a), two three-phase regions, $bcc + AlMo_3 + Al_8Mo_3$ and $\eta + \beta Al_8Cr_5 + liquid$ that were clearly identified in the three-phase alloys annealed at 1200 °C are well reproduced by the thermodynamic parameters in isothermal section. Three three-phase regions, $bcc + \beta Al_8Cr_5 + Al_8Mo_3$, $\eta + \beta Al_8Cr_5 + Al_8Mo_3$, and $\eta + Al_8Mo_3 + liquid$ were obtained from the calculated results. Two three-phase regions of $bcc + AlMo_3 + Al_8Mo_3$ and $\eta + \alpha Al_8Cr_5 + Al_8Mo_3$ were determined at 1000 °C, as shown in Fig. 6(b). Six three-phase regions, $bcc + \alpha Al_8Cr_5 + Al_8Mo_3$, $Al_4Cr + \alpha Al_8Cr_5 + liquid$, $\eta + \alpha Al_8Cr_5 + liquid$, $\eta + Al_8Mo_3 + liquid$, $Al_8Mo_3 + Al_4Mo + liquid$, and $Al_8Mo_3 + Al_4Mo + Al_3Mo$ were obtained from the thermodynamic calculation.

From the calculated results, the solid solubility ranges of Al and Mo in the η phase are about 75.32 and 14.82 ∼ 15.33 at.% at 1200 °C, respectively. While at 1000 °C, the ranges are 75.21 ∼ 76.50 at.% and 10.22 ∼ 12.16 at.%, respectively. With the decrease of temperature, its phase region becomes wider. The maximum solid solubility of Cr in the $AlMo_3$ phase is about 20.31 and 25.26 at.% at 1200 and 1000 °C, respectively, manifesting that the solubility of Cr in the $AlMo_3$ phase decreases with the increase of temperature. The solid solubility of Mo in the βAl_8Cr_5 phase at 1200 °C and the αAl_8Cr_5 phase at 1000 °C reaches about 14.57 and 34.34 at.%, respectively.

As shown in Fig. 7, the vertical sections of the Al-Cr-Mo system at 20% Al, 40 at.% Al, 10 at.% Cr, 24 at.% Cr, 30 at.% Mo, and 50 at.% Mo were calculated and plotted with the experimental data, to ensure the consistency of the optimized thermodynamic parameters in Table 4. The calculated results are in good agreement with the experimental information.

According to the obtained thermodynamic parameters, the predicted isothermal sections of the Al-Cr-Mo ternary system at 1400 and 800 °C are shown in Fig. 8(a)-(b). It is known that the βAl_8Cr_5 phase is stable temperature range of 1060 ∼ 1320 °C in the binary system.[26] However, the βAl_8Cr_5 phase is present at 1400 °C isothermal section in the Al-Cr-Mo ternary system, as shown in Fig. 8(b),

Table 4 Thermodynamic parameters in the Al-Cr-Mo ternary system optimized in this work

Phase	Parameters	References
liquid	$(Al,Cr,Mo)_1$	
	$^0L_{Al,Cr}^{Liquid} = -37139.1 + 2.0110T$	(Ref [26])
	$^1L_{Al,Cr}^{Liquid} = -15698.7 + 7.4555T$	(Ref [26])
	$^0L_{Al,Mo}^{Liquid} = -96235.7 + 20.9416T$	(Ref [27])
	$^1L_{Al,Mo}^{Liquid} = -4384.1 + 12.3636T$	(Ref [27])
	$^2L_{Al,Mo}^{Liquid} = -25091.6$	(Ref [27])
	$^0L_{Cr,Mo}^{Liquid} = 15810 - 6.714T$	(Ref [28])
	$^1L_{Cr,Mo}^{Liquid} = -6220$	(Ref [28])
	$^0L_{Al,Cr,Mo}^{Liquid} = -581900 + 300T$	This work
	$^1L_{Al,Cr,Mo}^{Liquid} = 209125 - 125T$	This work
	$^2L_{Al,Cr,Mo}^{Liquid} = 177300 - 100T$	This work
bcc	$(Al,Cr,Mo)_1$	
	$^0L_{Al,Cr}^{bcc} = -58257.5 + 8.4407T$	(Ref [26])
	$^0L_{Al,Mo}^{bcc} = -75938.8 + 10.8187T$	(Ref [27])
	$^1L_{Al,Mo}^{bcc} = -44502.8 + 21.6488T$	(Ref [27])
	$^2L_{Al,Mo}^{bcc} = -22927.1$	(Ref [27])
	$^0L_{Cr,Mo}^{bcc} = 28890 - 7.962T$	(Ref [28])
	$^1L_{Cr,Mo}^{bcc} = 5974 - 2.428T$	(Ref [28])
	$^0L_{Al,Cr,Mo}^{bcc} = 0$	This work
	$^1L_{Al,Cr,Mo}^{bcc} = -43810 - 30T$	This work
	$^2L_{Al,Cr,Mo}^{bcc} = 87300 - 100T$	This work
βAl_8Cr_5	$(Al,Cr,Mo)_8(Al,Cr,Mo)_5$	
	$^0G_{Al:Cr}^{\beta Al_8Cr_5} = 8{^0G_{Al}^{HSER}} + 5{^0G_{Cr}^{HSER}} - 238114.8$	(Ref [26])
	$^0G_{Al:Al}^{\beta Al_8Cr_5} = 13{^0G_{Al}^{HSER}} + 40000$	(Ref [26])
	$^0G_{Cr:Cr}^{\beta Al_8Cr_5} = 13{^0G_{Cr}^{HSER}} + 40000$	(Ref [26])
	$^0G_{Cr:Al}^{\beta Al_8Cr_5} = 8{^0G_{Cr}^{HSER}} + 5{^0G_{Al}^{HSER}} + 318114.8$	(Ref [26])
	$^0G_{Al:Al,Cr}^{\beta Al_8Cr_5} = 198488 - 236.4091T$	(Ref [26])
	$^1G_{Al:Al,Cr}^{\beta Al_8Cr_5} = -254728.3 + 98.3046T$	(Ref [26])
	$^0G_{Cr:Al,Cr}^{\beta Al_8Cr_5} = 198488 - 236.4091T$	(Ref [26])
	$^1G_{Cr:Al,Cr}^{\beta Al_8Cr_5} = -254728.3 + 98.3046T$	(Ref [26])
	$^0G_{Al,Cr:Al}^{\beta Al_8Cr_5} = 194038.6 - 57.0982T$	(Ref [26])
	$^1G_{Al,Cr:Al}^{\beta Al_8Cr_5} = 16289.5 - 99.3751T$	(Ref [26])
	$^0G_{Al,Cr:Cr}^{\beta Al_8Cr_5} = 194038.6 - 57.0982T$	(Ref [26])
	$^1G_{Al,Cr:Cr}^{\beta Al_8Cr_5} = 16289.5 - 99.3751T$	(Ref [26])
	$^0G_{Mo:Al}^{\beta Al_8Cr_5} = 8{^0G_{Mo}^{HSER}} + 5{^0G_{Al}^{HSER}}$	This work
	$^0G_{Mo:Cr}^{\beta Al_8Cr_5} = 100000 + 8{^0G_{Mo}^{HSER}} + 5{^0G_{Cr}^{HSER}}$	This work
	$^0G_{Al:Mo}^{\beta Al_8Cr_5} = -42635 - 5T + 8{^0G_{Al}^{HSER}} + 5{^0G_{Mo}^{HSER}}$	This work
	$^0G_{Cr:Mo}^{\beta Al_8Cr_5} = 100000 + 8{^0G_{Cr}^{HSER}} + 5{^0G_{Mo}^{HSER}}$	This work

28

J. Phase Equilib. Diffus. (2024) 45:18–35

Table 4 continued

Phase	Parameters	References
	$^0G_{Mo:Mo}^{\beta Al_8 Cr_5} = 70000 + 13\,^0G_{Mo}^{HSER}$	This work
	$^0L_{Al:Cr,Mo}^{\beta Al_8 Cr_5} = -389525 - 75T$	This work
	$^1L_{Al:Cr,Mo}^{\beta Al_8 Cr_5} = 350950 - 150T$	This work
	$^0L_{Al:Al,Cr,Mo}^{\beta Al_8 Cr_5} = -541750 - 250T$	This work
$\alpha Al_8 Cr_5$	$(Al,Cr,Mo)_8(Al,Cr,Mo)_5$	
	$^0G_{Al:Cr}^{\alpha Al_8 Cr_5} = 8\,^0G_{Al}^{HSER} + 5\,^0G_{Cr}^{HSER}$ $-252507.8 + 10.3963T$	(Ref 26)
	$^0G_{Al:Al}^{\alpha Al_8 Cr_5} = 13\,^0G_{Al}^{HSER} + 40000$	(Ref 26)
	$^0G_{Cr:Cr}^{\alpha Al_8 Cr_5} = 13\,^0G_{Cr}^{HSER} + 40000$	(Ref 26)
	$^0G_{Cr:Al}^{\alpha Al_8 Cr_5} = 5\,^0G_{Al}^{HSER} + 8\,^0G_{Cr}^{HSER}$ $+332507.8 - 10.3963T$	(Ref 26)
	$^0G_{Al:Al,Cr}^{\alpha Al_8 Cr_5} = -302291.9 + 156.9409T$	(Ref 26)
	$^1G_{Al:Al,Cr}^{\alpha Al_8 Cr_5} = -84584.3$	(Ref 26)
	$^0G_{Cr:Al,Cr}^{\alpha Al_8 Cr_5} = -302291.9 + 156.9409T$	(Ref 26)
	$^1G_{Cr:Al,Cr}^{\alpha Al_8 Cr_5} = -84584.3$	(Ref 26)
	$^0G_{Al,Cr:Al}^{\alpha Al_8 Cr_5} = 140019.3 + 2.7138T$	(Ref 26)
	$^1G_{Al,Cr:Al}^{\alpha Al_8 Cr_5} = -298819.0 + 92.8656T$	(Ref 26)
	$^0G_{Al,Cr:Cr}^{\alpha Al_8 Cr_5} = 140019.3 + 2.7138T$	(Ref 26)
	$^1G_{Al,Cr:Cr}^{\alpha Al_8 Cr_5} = -298819.0 + 92.8656T$	(Ref 26)
	$^0G_{Mo:Al}^{\alpha Al_8 Cr_5} = 8\,^0G_{Mo}^{HSER} + 5\,^0G_{Al}^{HSER}$	This work
	$^0G_{Mo:Cr}^{\alpha Al_8 Cr_5} = 100000 + 8\,^0G_{Mo}^{HSER} + 5\,^0G_{Cr}^{HSER}$	This work
	$^0G_{Al:Mo}^{\alpha Al_8 Cr_5} = -50000 + 8\,^0G_{Al}^{HSER} + 5\,^0G_{Mo}^{HSER}$	This work
	$^0G_{Cr:Mo}^{\alpha Al_8 Cr_5} = 100000 + 8\,^0G_{Cr}^{HSER} + 5\,^0G_{Mo}^{HSER}$	This work
	$^0G_{Mo:Mo}^{\alpha Al_8 Cr_5} = 70000 + 13\,^0G_{Mo}^{HSER}$	This work
	$^0L_{Al:Cr,Mo}^{\alpha Al_8 Cr_5} = -384000$	This work
	$^0L_{Al:Al,Cr,Mo}^{\alpha Al_8 Cr_5} = -1545550 + 350T$	This work
$Al_7 Cr$	$(Al)_7(Al,Cr)_1$	
	$^0G_{Al:Cr}^{Al_7 Cr} = -100970 + 23.5612T$ $+7\,^0G_{Al}^{HSER} + ^0G_{Cr}^{HSER}$	(Ref 26)
	$^0G_{Al:Al}^{Al_7 Cr} = 24074.5 + 8\,^0G_{Al}^{HSER}$	(Ref 26)
	$^0G_{Al:Al,Cr}^{Al_7 Cr} = -21094.1 + 12.6986T$	(Ref 26)
$Al_{11}Cr_2$	$(Al)_{11}(Al,Cr)_2$	
	$^0G_{Al:Cr}^{Al_{11}Cr_2} = -145700.9$ $+11\,^0G_{Al}^{HSER} + 2\,^0G_{Cr}^{HSER}$	(Ref 26)
	$^0G_{Al:Al}^{Al_{11}Cr_2} = 30000 + 13\,^0G_{Al}^{HSER}$	(Ref 26)
	$^0G_{Al:Al,Cr}^{Al_{11}Cr_2} = -21094.1 + 12.6986T$	(Ref 26)
$Al_4 Cr$	$(Al)_4(Al,Cr)_1$	
	$^0G_{Al:Cr}^{Al_4 Cr} = -79750 + 9.8532T$ $+4\,^0G_{Al}^{HSER} + ^0G_{Cr}^{HSER}$	(Ref 26)

Table 4 continued

Phase	Parameters	References
	$^0G_{Al:Al}^{Al_4Cr} = 25868.2 + 5\,^0G_{Al}^{HSER}$	(Ref [26])
	$^0G_{Al:Al,Cr}^{Al_4Cr} = -71625 + 53.003T$	(Ref [26])
AlCr$_2$	(Al,Cr)(Al,Cr)$_2$	
	$^0G_{Al:Cr}^{AlCr_2} = -45279.2 + \,^0G_{Al}^{HSER} + 2\,^0G_{Cr}^{HSER}$	(Ref [26])
	$^0G_{Cr:Al}^{AlCr_2} = 75279.2 + \,^0G_{Cr}^{HSER} + 2\,^0G_{Al}^{HSER}$	(Ref [26])
	$^0G_{Al:Al}^{AlCr_2} = 15000 + 3\,^0G_{Al}^{HSER}$	(Ref [26])
	$^0G_{Cr:Cr}^{AlCr_2} = 15000 + 3\,^0G_{Cr}^{HSER}$	(Ref [26])
	$^0G_{Al:Al,Cr}^{AlCr_2} = -31502.4 + 5.7033T$	(Ref [26])
	$^0G_{Cr:Al,Cr}^{AlCr_2} = -31502.4 + 5.7033T$	(Ref [26])
	$^0G_{Al,Cr:Al}^{AlCr_2} = -11282.4 - 6.37T$	(Ref [26])
	$^0G_{Al,Cr:Cr}^{AlCr_2} = -11282.4 - 6.37T$	(Ref [26])
Al$_8$Mo$_3$	(Al)$_8$(Cr,Mo)$_5$	
	$^0G_{Al:Mo}^{Al_8Mo_3} = -432556.9 + 99.1737T$ $+ 8\,^0G_{Al}^{HSER} + 3\,^0G_{Cr}^{HSER}$	(Ref [27])
	$^0G_{Al:Cr}^{Al_8Mo_3} = -8000 + 8\,^0G_{Al}^{HSER} + 3\,^0G_{Cr}^{HSER}$	This work
	$^0L_{Al:Cr,Mo}^{Al_8Mo_3} = -337300 + 100T$	This work
AlMo$_3$	(Al,Mo)$_1$(Al,Cr,Mo)$_3$	
	$^0G_{Al:Al}^{AlMo_3} = 20000 + 4\,^0G_{Al}^{HSER}$	(Ref [27])
	$^0G_{Al:Mo}^{AlMo_3} = -95830.9 + 2.0081T$ $+ \,^0G_{Al}^{HSER} + 3\,^0G_{Mo}^{HSER}$	(Ref [27])
	$^0G_{Mo:Al}^{AlMo_3} = 135830.9 - 2.0081T$ $+ \,^0G_{Mo}^{HSER} + 3\,^0G_{Al}^{HSER}$	(Ref [27])
	$^0G_{Mo:Mo}^{AlMo_3} = 20000 + 4\,^0G_{Mo}^{HSER}$	(Ref [27])
	$^0G_{Al,Mo:Al}^{AlMo_3} = 11628.1$	(Ref [27])
	$^0G_{Al,Mo:Mo}^{AlMo_3} = 11628.1$	(Ref [27])
	$^0G_{Al:Al,Mo}^{AlMo_3} = 52100$	(Ref [27])
	$^0G_{Mo:Al,Mo}^{AlMo_3} = 52100$	(Ref [27])
	$^0G_{Al:Cr}^{AlMo_3} = -21365 + 5T + \,^0G_{Al}^{HSER} + 3\,^0G_{Cr}^{HSER}$	This work
	$^0G_{Mo:Cr}^{AlMo_3} = 19000 + \,^0G_{Mo}^{HSER} + 3\,^0G_{Cr}^{HSER}$	This work
	$^0L_{Al,Mo:Cr}^{AlMo_3} = -17365 + 5T$	This work
	$^0L_{Al:Mo,Cr}^{AlMo_3} = -71555 + 35T$	This work
	$^0L_{Al:Al,Mo,Cr}^{AlMo_3} = -604600 + 200T$	This work
Al$_{12}$Mo	(Al)$_{12}$(Mo)$_1$	
	$^0G_{Al:Mo}^{Al_{12}Mo} = -146766.8 + 23.1256T$ $+ 12\,^0G_{Al}^{HSER} + \,^0G_{Mo}^{HSER}$	(Ref [27])
Al$_4$Mo	(Al)$_4$(Mo)$_1$	
	$^0G_{Al:Mo}^{Al_4Mo} = -138851.8 + 23.112T$ $+ 4\,^0G_{Al}^{HSER} + \,^0G_{Mo}^{HSER}$	(Ref [27])
Al$_3$Mo	(Al)$_3$(Mo)$_1$	
	$^0G_{Al:Mo}^{Al_3Mo} = -143196.7 + 30.6912T$ $+ 3\,^0G_{Al}^{HSER} + \,^0G_{Mo}^{HSER}$	(Ref [27])

Table 4 continued

Phase	Parameters	References
Al$_{17}$Mo$_4$	(Al)$_{17}$(Mo)$_4$	
	$^0G_{Al:Mo}^{Al_{17}Mo_4} = -578455.4 + 107.4145T$ $+17\,^0G_{Al}^{HSER} + 4\,^0G_{Mo}^{HSER}$	(Ref 27)
Al$_{22}$Mo$_5$	(Al)$_{22}$(Mo)$_5$	
	$^0G_{Al:Mo}^{Al_{22}Mo_5} = -723273.3 + 132.3154T$ $+22\,^0G_{Al}^{HSER} + 5\,^0G_{Mo}^{HSER}$	(Ref 27)
Al$_5$Mo	(Al)$_5$(Mo)$_1$	
	$^0G_{Al:Mo}^{Al_5Mo} = -144819.3 + 25.4357T$ $+5\,^0G_{Al}^{HSER} + \,^0G_{Mo}^{HSER}$	(Ref 27)
Al$_{63}$Mo$_{37}$	(Al)$_{63}$(Mo)$_{37}$	
	$^0G_{Al:Mo}^{Al_{63}Mo_{37}} = -1638310.2 - 403.7604T$ $+63\,^0G_{Al}^{HSER} + 37\,^0G_{Mo}^{HSER}$	(Ref 27)
η	(Al)$_3$(Al,Cr,Mo)$_1$	
	$^0G_{Al:Cr}^{\eta} = 3\,^0G_{Al}^{HSER} + \,^0G_{Cr}^{HSER}$	This work
	$^0G_{Al:Mo}^{\eta} = 3\,^0G_{Al}^{HSER} + \,^0G_{Mo}^{HSER}$	This work
	$^0G_{Al:Al}^{\eta} = 20000 + 4\,^0G_{Al}^{HSER}$	This work
	$^0L_{Al:Cr,Mo}^{\eta} = -486760 + 120T$	This work
	$^1L_{Al:Cr,Mo}^{\eta} = 537040 - 480T$	This work
	$^2L_{Al:Cr,Mo}^{\eta} = -73620 - 60T$	This work
	$^0L_{Al:Al,Cr,Mo}^{\eta} = -434000$	This work

indicating that the addition of Mo with high melting temperature stabilizes the βAl$_8$Cr$_5$ phase at higher temperature. At 800 °C the isothermal section shows that the η phase is still stable and the bcc phase has separated into bcc1 (Cr) and bcc2 (Mo).

The calculated liquidus projection of the entire composition range with the published experimental data[22] and the enlarged Al-rich corner of the Al-Cr-Mo ternary system are presented in Fig. 9(a)-(b). It should be noted that inferring from the Al-Cr binary system,[31] the AlCr$_2$ phase precipitates from the bcc phase rather than the liquid phase. Therefore, the alloy of Al$_{33}$Cr$_{60}$Mo$_7$, which precipitated the AlCr$_2$ phase was not considered in this calculation. The complete invariant reaction scheme obtained is shown in Fig. 10. Since experimental data for the liquidus reactions are limited, further experimental investigations are needed for determining the actual reaction scheme.

As shown in Fig. 1(c), the miscibility gap of the bcc phase exists below 941 °C in the Cr-Mo binary system.[28] The effect of Al addition on the miscibility gap of the bcc phase in the Al-Cr-Mo system can be evaluated according to the obtained thermodynamic parameters. Fig. 11 shows the miscibility gap of the bcc phase in the Al-Cr-Mo ternary system, which only exists on the Cr-Mo side and

the bcc phase separation extends from Cr-Mo side to Al side with decreasing temperature. The tie-lines in the Al-Cr-Mo system lie along the AlCr-AlMo direction. This can be reasonably explained by the enthalpy of mixing in the Al-Cr, Al-Mo, and Cr-Mo binary systems. Based on the report of Takeuchi et al.(Ref 32), the mixing enthalpies in the Al-Cr, Al-Mo, and Cr-Mo systems are –10, –5, and 0 kJ/mol, respectively. Accordingly, with the enthalpy of mixing between Cr and Mo being equal to 0, this basically an ideal solution. Therefore, there is an infinite solid solution bcc phase with a very large composition and temperature range in the Cr-Mo binary system. However, Kubaschewski et al.(Ref 33) experimentally measured that there is a large two-phase separation of bcc phase in the Cr-Mo binary system in the temperature range below 941 °C, indicating that the atoms of Cr and Mo were mutually repulsive below 941 °C, and the enthalpy of mixing between Cr and Mo was positive.[28, 34] The enthalpy of mixing between Al-Mo and Al-Cr is negative, which means that attractive forces exist between Al and Cr, and Al and Mo, the tie-line radiate from the Al-Cr side to the Al-Mo side.

The calculated miscibility gap of the bcc phase in the Al-Cr-Mo system with different Al additions is shown in
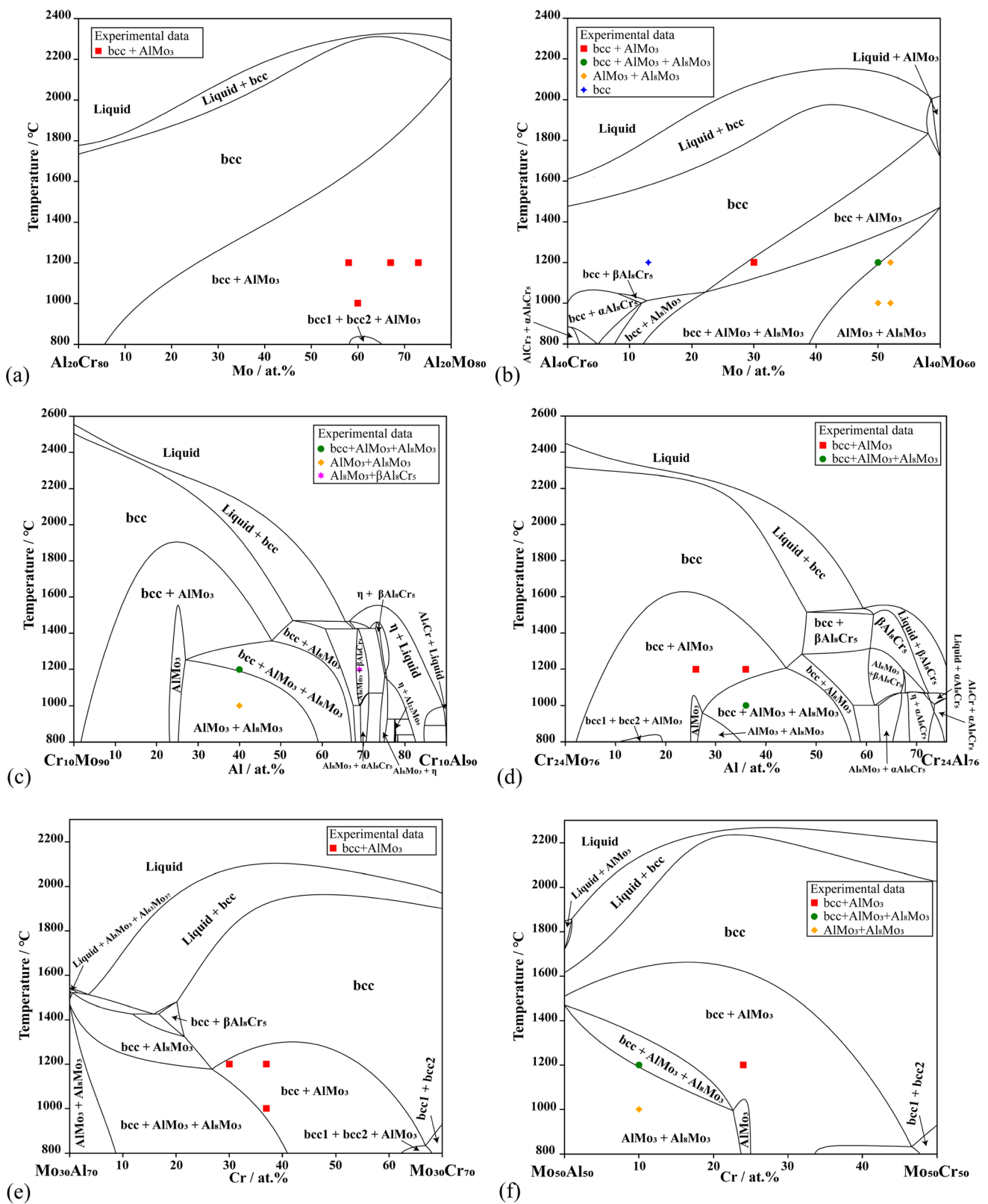
Fig. 7 Calculated vertical sections of the Al-Cr-Mo system at (a) 20 at.% Al, (b) 40 at.% Al, (c) 10 at.% Cr, (d) 24 at.% Cr, (e) 30 at.% Mo, and (f) 50 at.% Mo with the experimental data from the present work
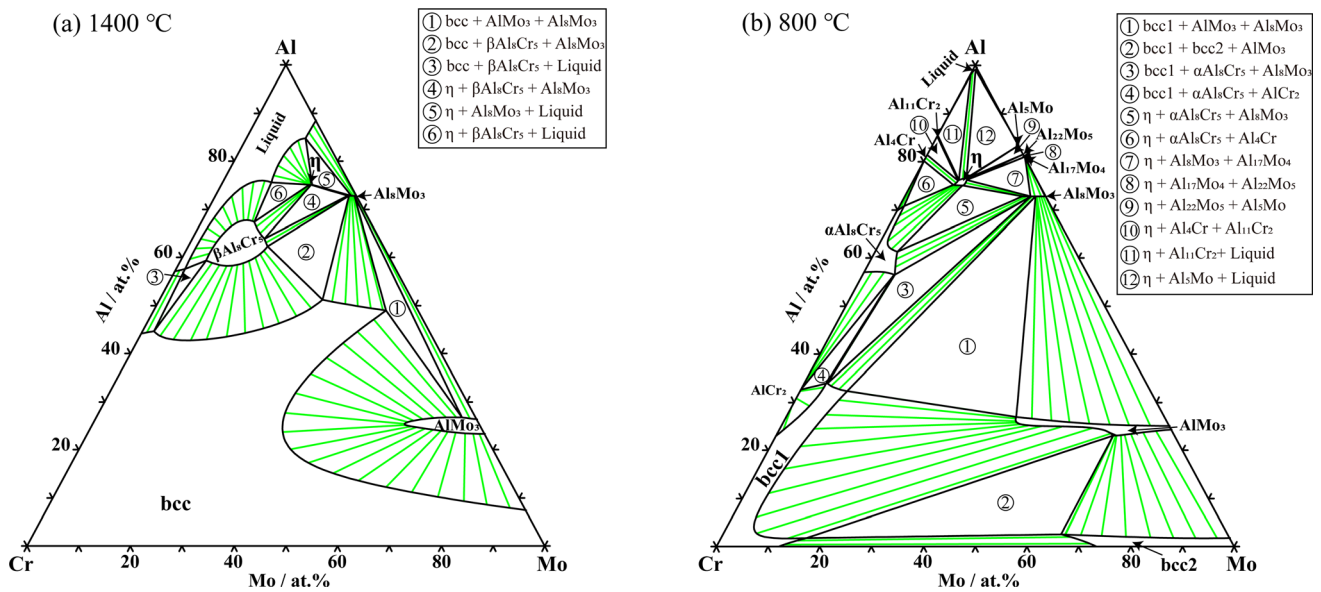
32

J. Phase Equilib. Diffus. (2024) 45:18–35

Fig. 8 Predicted isothermal sections of the Al-Cr-Mo system at (a) 1400 °C and (b) 800 °C
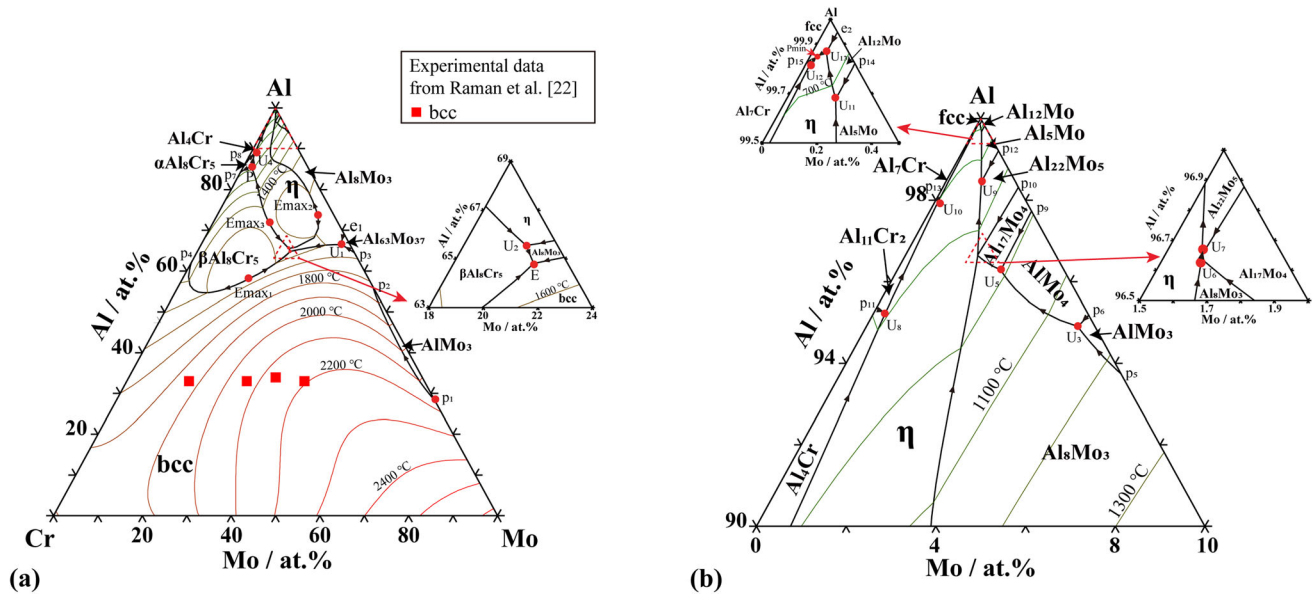

Fig. 9 Calculated liquidus projection of the Al-Cr-Mo system with isothermal lines: (a) over the whole composition range with experimental data from (Ref 22) and (b) Al-rich corner

Fig. 12, where the critical temperature gradually decreases with the increasing amount of Al, and the alloy composition corresponding to the critical temperature moves towards the Mo-rich side. This phenomenon manifests that Al additions can significantly decrease the bcc phase separation.sss

5 Conclusions

In this study, isothermal sections of the Al-Cr-Mo ternary system at 1200 and 1000 °C were experimentally investigated and thermodynamically described. From the obtained results, the following conclusions can be drawn:

(1)   Six primary phases, bcc, AlMo$_3$, Al$_8$Cr$_5$, βAl$_8$Cr$_5$, αAl$_8$Cr$_5$, and liquid were experimentally determined. Besides, a new ternary phase η with AlTi$_3$-type crystal structure covering a composition range
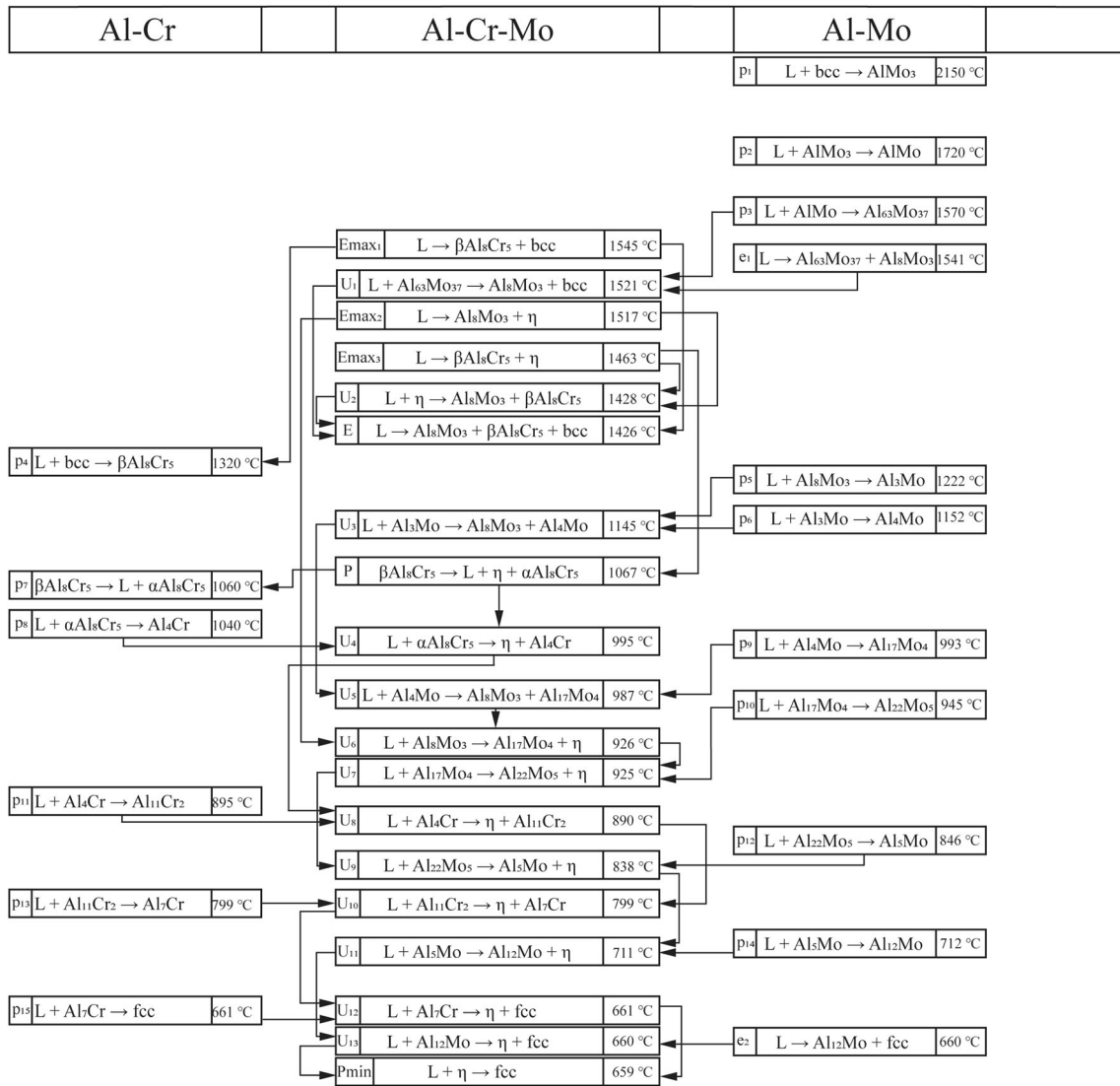
Al-Cr	Al-Cr-Mo	Al-Mo

Al-Mo:
- p_1 | L + bcc → AlMo$_3$ | 2150 °C
- p_2 | L + AlMo$_3$ → AlMo | 1720 °C
- p_3 | L + AlMo → Al$_{63}$Mo$_{37}$ | 1570 °C
- e_1 | L → Al$_{63}$Mo$_{37}$ + Al$_8$Mo$_3$ | 1541 °C
- p_5 | L + Al$_8$Mo$_3$ → Al$_3$Mo | 1222 °C
- p_6 | L + Al$_3$Mo → Al$_4$Mo | 1152 °C
- p_9 | L + Al$_4$Mo → Al$_{17}$Mo$_4$ | 993 °C
- p_{10} | L + Al$_{17}$Mo$_4$ → Al$_{22}$Mo$_5$ | 945 °C
- p_{12} | L + Al$_{22}$Mo$_5$ → Al$_5$Mo | 846 °C
- p_{14} | L + Al$_5$Mo → Al$_{12}$Mo | 712 °C
- e_2 | L → Al$_{12}$Mo + fcc | 660 °C

Al-Cr-Mo:
- $Emax_1$ | L → βAl$_8$Cr$_5$ + bcc | 1545 °C
- U_1 | L + Al$_{63}$Mo$_{37}$ → Al$_8$Mo$_3$ + bcc | 1521 °C
- $Emax_2$ | L → Al$_8$Mo$_3$ + η | 1517 °C
- $Emax_3$ | L → βAl$_8$Cr$_5$ + η | 1463 °C
- U_2 | L + η → Al$_8$Mo$_3$ + βAl$_8$Cr$_5$ | 1428 °C
- E | L → Al$_8$Mo$_3$ + βAl$_8$Cr$_5$ + bcc | 1426 °C
- U_3 | L + Al$_3$Mo → Al$_8$Mo$_3$ + Al$_4$Mo | 1145 °C
- P | βAl$_8$Cr$_5$ → L + η + αAl$_8$Cr$_5$ | 1067 °C
- U_4 | L + αAl$_8$Cr$_5$ → η + Al$_4$Cr | 995 °C
- U_5 | L + Al$_4$Mo → Al$_8$Mo$_3$ + Al$_{17}$Mo$_4$ | 987 °C
- U_6 | L + Al$_8$Mo$_3$ → Al$_{17}$Mo$_4$ + η | 926 °C
- U_7 | L + Al$_{17}$Mo$_4$ → Al$_{22}$Mo$_5$ + η | 925 °C
- U_8 | L + Al$_4$Cr → η + Al$_{11}$Cr$_2$ | 890 °C
- U_9 | L + Al$_{22}$Mo$_5$ → Al$_5$Mo + η | 838 °C
- U_{10} | L + Al$_{11}$Cr$_2$ → η + Al$_7$Cr | 799 °C
- U_{11} | L + Al$_5$Mo → Al$_{12}$Mo + η | 711 °C
- U_{12} | L + Al$_7$Cr → η + fcc | 661 °C
- U_{13} | L + Al$_{12}$Mo → η + fcc | 660 °C
- $Pmin$ | L + η → fcc | 659 °C

Al-Cr:
- p_4 | L + bcc → βAl$_8$Cr$_5$ | 1320 °C
- p_7 | βAl$_8$Cr$_5$ → L + αAl$_8$Cr$_5$ | 1060 °C
- p_8 | L + αAl$_8$Cr$_5$ → Al$_4$Cr | 1040 °C
- p_{11} | L + Al$_4$Cr → Al$_{11}$Cr$_2$ | 895 °C
- p_{13} | L + Al$_{11}$Cr$_2$ → Al$_7$Cr | 799 °C
- p_{15} | L + Al$_7$Cr → fcc | 661 °C

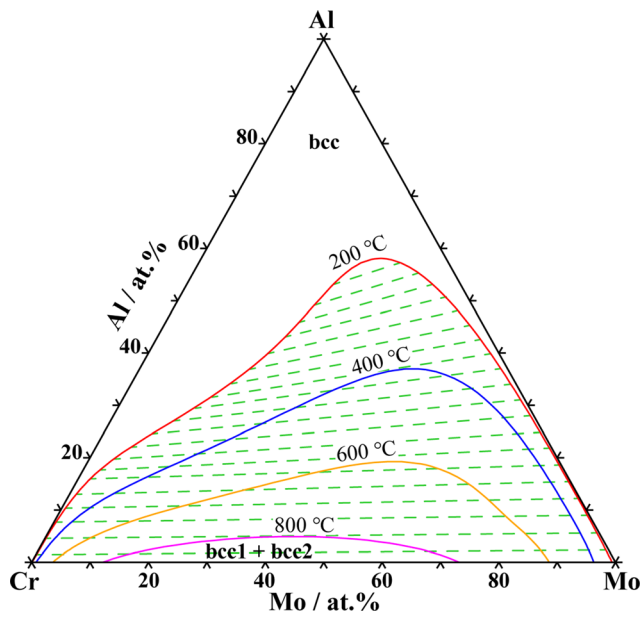Fig. 10 Invariant reaction scheme of the Al-Cr-Mo system

Fig. 11 Calculated miscibility gap of the bcc phase in the Al-Cr-Mo system
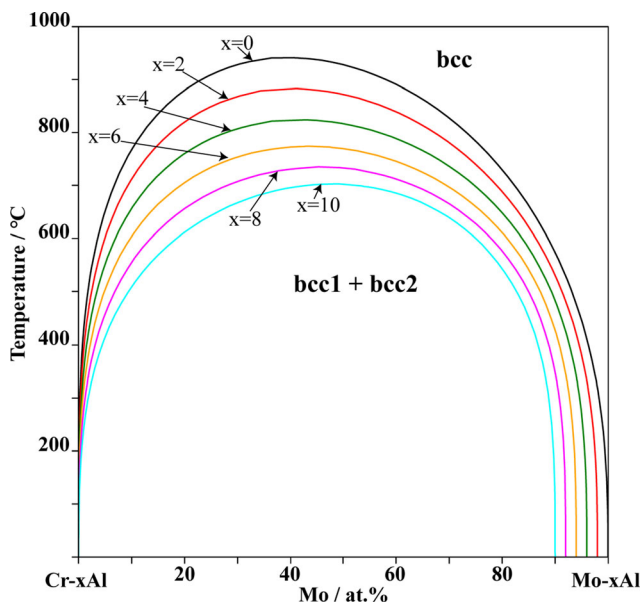

Fig. 12 Calculated miscibility gap of bcc phase in the Al-Cr-Mo system with different Al additions

near ∼ 75 at.% Al was detected in these two isothermal sections for the first time.

(2) The Al-Cr-Mo ternary system was thermodynamically assessed in the present work using the CALPHAD method based on the available experimental data. A set of thermodynamic parameters for the Al-Cr-Mo system was obtained. The calculated isothermal and vertical sections are in good agreement with most of the reliable experimental data. The liquidus projection and reaction scheme of the

Al-Cr-Mo system over the whole composition are presented. The calculated miscibility gap of the bcc phase in the Al-Cr-Mo ternary system is also presented.

Conflict of interest The authors declare that they have no known competing financial interests or personal relationships that could have appeared to influence the work reported in this paper.

References

1. P. Caron, High γ' Solvus New Generation Nickel-Based Superalloys for Single Crystal Turbine Blade Applications, *Superalloys*, 2000, **2000**, p 737–746.
2. H. Fecht and D. Furrer, Processing of Nickel-Base Superalloys for Turbine Engine Disc Applications, *Adv. Eng. Mater.*, 2000, **2**(12), p 777–787.
3. T. Murakumo, T. Kobayashi, Y. Koizumi, and H. Harada, Creep Behaviour of Ni-Base Single-Crystal Superalloys with Various γ' Volume Fraction, *Acta Mater.*, 2004, **52**(12), p 3737–3744.
4. T.M. Pollock and S. Tin, Nickel-Based Superalloys for Advanced Turbine Engines: Chemistry, Microstructure and Properties, *J. Propuls. Power*, 2006, **22**(2), p 361–374.
5. R.C. Reed, *The Superalloys: Fundamentals and Applications*. Cambridge University Press, Cambridge, 2006.
6. Y.Y. Qiu, Effect of the Al and Mo on the Lattice Mismatch and γ' Morphology in Ni-Based Superalloys, *Scr. Metall. Mater.*, 1995, **33**(12), p 1961–1968.
7. X. Lu, S. Tian, X. Yu, and C. Wang, Oxidation Behavior of a Single-crystal Ni-base Superalloy in Air at 900 and 1050 °C, *Rare Met.*, 2011, **30**(S1), p 439–442.
8. H. Long, S. Mao, Y. Liu, Z. Zhang, and X. Han, Microstructural and Compositional Design of Ni-Based Single Crystalline Superalloys - A Review, *J. Alloys Compd.*, 2018, **743**, p 203–220.
9. B. Wang, J. Zhang, T. Huang, H. Su, Z. Li, L. Liu, and H. Fu, Influence of W, Re, Cr, and Mo on Microstructural Stability of the Third Generation Ni-Based Single Crystal Superalloys, *J. Mater. Res.*, 2016, **31**(21), p 3381–3389.
10. S.J. Park, S.M. Seo, Y.S. Yoo, H.W. Jeong, and H. Jang, Effects of Cr, W, and Mo on the High Temperature Oxidation of Ni-Based Superalloys, *Materials*, 2019, **12**(18), p 2934.
11. J.Y. Chen, Q. Feng, L.M. Cao, and Z.Q. Sun, Improvement of Stress-Rupture Property by Cr Addition in Ni-Based Single Crystal Superalloys, *Mater. Sci. Eng. A*, 2011, **528**(10), p 3791–3798.
12. Q. Shi, J. Huo, Y. Zheng, and Q. Feng, Influence of Mo and Ru Additions on the Creep Behavior of Ni-Based Single Crystal Superalloys at 1100 °C, *Mater. Sci. Eng. A*, 2018, **725**, p 148–159.
13. B. Seiser, R. Drautz, and D.G. Pettifor, TCP Phase Predictions in Ni-Based Superalloys: Structure Maps Revisited, *Acta Mater.*, 2011, **59**(2), p 749–763.
14. Q. Yu, C. Wang, G. Yang, Y. Ren, N. Liu, Y. Liang, and C. Dong, Influence of Cr/Mo Ratio on Microstructure and Mechanical Properties of the Ni-Based Superalloys Fabricated by Laser Additive Manufacturing, *J. Alloys Compd.*, 2022, **894**, p 162484.

J. Phase Equilib. Diffus. (2024) 45:18–35

35

15. B. Grushko, W. Kowalski, D. Pavlyuchkov, B. Przepiórzyński, and M. Surowiec, A Contribution to the Al-Ni-Cr Phase Diagram, *J. Alloys Compd.*, 2008, **460**(1), p 299–304.

16. Y. Wang and G. Cacciamani, Thermodynamic Modeling of the Al-Cr-Ni System over the Entire Composition and Temperature Range, *J. Alloys Compd.*, 2016, **688**, p 422–435.

17. P.E.A. Turchi, L. Kaufman, and Z.K. Liu, Modeling of Ni-Cr-Mo Based Alloys: Part I—Phase Stability, *Calphad*, 2006, **30**(1), p 70–87.

18. J. Peng. Experimental Investigation and Thermodynamic Modeling of the Al-Cr-Mo-Ni System and Its Sub-Systems, Karlsruher Instituts für Technologie, 2016.

19. X. Lu, Y. Cui, and Z. Jin, Experimental and Thermodynamic Investigation of the Ni-Al-Mo System, *Metall. Mater. Trans. A*, 1999, **30**(7), p 1785–1795.

20. S.H. Zhou, Y. Wang, L.Q. Chen, Z.K. Liu, and R.E. Napolitano, Solution-Based Thermodynamic Modeling of the Ni-Al-Mo System Using First-Principles Calculations, *Calphad*, 2014, **46**, p 124–133.

21. J. Peng, P. Franke, D. Manara, T. Watkins, R.J.M. Konings, and H.J. Seifert, Experimental Investigation and Thermodynamic Re-Assessment of the Al-Mo-Ni System, *J. Alloys Compd.*, 2016, **674**, p 305–314.

22. A. Raman and K. Schubert, Über die Verbreitung des Zr_2Cu-Type und Cr_2Al-Type, *Z. Fuer. Met.*, 1964, **55**(12), p 798–804.

23. L. Kaufman and H. Nesor, Calculation of Superalloy Phase Diagrams: Part II, *Metall. Mater. Trans. B*, 1974, **5**(7), p 1623–1629.

24. J. Peng, P. Franke, and H.J. Seifert, Experimental Investigation and CALPHAD Assessment of the Eutectic Trough in the System NiAl-Cr-Mo, *J. Phase Equilib. Diffus.*, 2016, **37**(5), p 592–600.

25. A.T. Dinsdale, SGTE Data for Pure Elements, *Calphad*, 1991, **15**(4), p 317–425.

26. Y. Liang, C. Guo, C. Li, and Z. Du, Thermodynamic Modeling of the Al-Cr System, *J. Alloys Compd.*, 2008, **460**(1), p 314–319.

27. Z. Du, C. Guo, C. Li, and W. Zhang, Thermodynamic Description of the Al-Mo and Al-Fe-Mo Systems, *J. Phase Equilib. Diffus.*, 2009, **30**(5), p 487–501.

28. K. Frisk and P. Gustafson, An Assessment of the Cr-Mo-W System, *Calphad*, 1988, **12**(3), p 247–254.

29. O. Redlich and A.T. Kister, Algebraic Representation of Thermodynamic Properties and the Classification of Solutions, *Ind. Eng. Chem.*, 1948, **40**(2), p 345–348.

30. M. Hillert, Empirical Methods of Predicting and Representing Thermodynamic Properties of Ternary Solution Phases, *Calphad*, 1980, **4**(1), p 1–12.

31. F. Stein, C. He, and I. Wossack, The Liquidus Surface of the Cr-Al-Nb System and Re-Investigation of the Cr-Nb and Al-Cr Phase Diagrams, *J. Alloys Compd.*, 2014, **598**, p 253–265.

32. A. Takeuchi and A. Inoue, Classification of Bulk Metallic Glasses by Atomic Size Difference, Heat of Mixing and Period of Constituent Elements and Its Application to Characterization of the Main Alloying Element, *Mater. Trans.*, 2005, **46**(12), p 2817–2829.

33. O. Kubaschewski and T.G. Chart, Calculation of Metallurgical Equilibrium Diagrams from Thermochemical Data, *J. Inst. Met.*, 1965, **93**, p 329–338.

34. M. Laffitte and O. Kubaschewski, Activities of Chromium in Chromium-Molybdenum Solid Solutions, *Trans. Faraday Soc.*, 1961, **57**(6), p 932–934.